Combustion Characteristics of Inverse Oxygen/Methane Coaxial Jet Flames at Elevated Pressure

Young Hoo Kim, Jae Hyun Kim and Oh Chae Kwon
Sungkyunkwan University
Suwon, Gyeonggi-do, Republic of Korea

1 Introduction

Oxygen (O_2)/hydrogen (H_2) and O_2/kerosene (RP-1) bipropellants have been widely used as a propellant of liquid rocket engines. Characteristics of H_2 as a fuel of rocket engines, such as the high specific impulse and no coking limit, are useful and thus it has been recently used for the Artemis I [1]. Also, RP-1 has been used due to its characteristics such as high propellant density which enables a compact design of rocket engines [2]. Meanwhile, there is a growing interest for O_2/methane (CH_4) bipropellants due to their characteristics such as low cost, in-situ resource utilization, higher coking limits and less soot formation which are important particularly for reusable rocket engines and thus there are several projects which are related to the O_2/CH_4 bipropellants, such as the Raptor engine of Space X [2–4]. Compared with the conventional liquid propellants such as H_2 and RP-1, however, the CH_4 propellants have not been used for commercial missions and space exploration yet, and thus their fundamental and practical studies for liquid rocket engines have been recently conducted, e.g., the combustion and flow characteristics of liquid oxygen (LO_2)/gaseous methane (GCH_4) bipropellants for various types of injectors and the flame anchoring characteristics of gaseous oxygen (GO_2)/GCH_4 bipropellants through flame and flow visualization [5,6]. However, further studies of the combustion characteristics of O_2/CH_4 bipropellants at various phases, including flame-turbulence interaction which is important for stable burning, are necessary to effectively design the rocket engines using the propellants.

Thus, the combustion characteristics of GO_2/GCH_4 have been investigated through the flame and flow visualization and compared with the GO_2/GH_2 in this laboratory [7–11]. Extending the previous studies that have been conducted for the upward injection of GO_2/GCH_4 in this laboratory, injection is changed to the downward injection which is the same as the real rocket engine condition in the present study, and we aim to investigate the combustion characteristics of GO_2/GCH_4 coaxial jet flames in a model combustion chamber at elevated combustion pressure, including flame-turbulence interaction and using the flame visualization such as OH^* chemiluminescence and OH-planar laser induced fluorescence (OH-PLIF) imaging.

2 Experimental Methods

Fig. 1a shows a schematic of the present experimental apparatus which was also used in the previous study [10] except a fuel supply line (CH_4 instead of H_2). A combustor (P50 combustor) is composed of

Correspondence to: okwon@skku.edu

an octagonal quartz-windowed combustion chamber, a coaxial shear injector, a torch ignitor, a pressure gauge (DPG3500; accuracy of ±1.0%) and a nozzle. The combustion chamber which has the internal volume of Φ60 × 244 mm^3 is designed to endure pressure up to 50 bars. Four quartz windows of 172.0 × 25.0 mm^2 are installed on the combustor for the flame visualization: a pair of the main optical quartz windows are installed on the front and back plates of the combustor to obtain flame images and a pair of the quartz windows on the side plates for a laser sheet. The coaxial shear injector is installed on the upstream end plate of the combustor without recess, which is composed of a center O_2 jet nozzle and an annulus CH_4 jet nozzle. The O_2 jet nozzle diameter is 2.00 mm, the O_2 jet nozzle post thickness is 0.40 mm, and the CH_4 jet nozzle diameter is 3.44 mm. For elevated combustion pressure (P_c) conditions, the exit nozzle with its diameter d_n = 1.0 mm is located at the downstream end plate of the combustor. Thus, a fully opened nozzle (i.e., no downstream end plate) is used for normal pressure (NP, 1.0 bar) and the nozzle with d_n = 1.0 mm for the elevated pressure up to 12.3 bar.

GO_2 and GCH_4 are supplied to the coaxial injector at normal temperature (NT, 298 ± 3 K) by commercial mass flow controllers (Porter 632M0ABD88V with ±2.0% accuracy of full scale) and ignited by the torch ignitor which is installed on the side plate of the combustor. After each test, gaseous nitrogen (GN_2) is injected through a purge line for venting the tested gases and cooling the combustor. The oxygen-to-fuel momentum flux ratio $(O/F)_{mom}$ is expected to be one of the major parameters for nonpremixed flame stability [12]. Selecting a fixed value of $(O/F)_{mom}$ = 6.0 which corresponds to an operating condition of the Raptor engine [13], experiments for inverse GO_2/GCH_4 coaxial jet nonpremixed flames at NT and P_c = 1.0–12.3 bar are conducted at various injection velocities.

To understand the structure of the coaxial jet flames of downward-injected GO_2/GCH_4 in the model combustion chamber at elevated combustion pressure, OH^* chemiluminescence and OH-PLIF images are obtained near the injector lip using an intensified charged-couple device (ICCD) camera (Oxford Instruments, Andor i-star 334T; resolution: 1024 × 1024 pixels) with an UV (ultraviolet) lens (Jenoptik CoastalOpt®, UV-VIS SLR, focal length: 105 mm) and a narrowband interference filter (WG-305 and UG-11) centered at 310 nm. The inverse Abel transform is applied to the line-of-sight (LOS) images of OH^* chemiluminescence which are obtained with the exposure time of 2 and 10 ms for providing planar images [14]. Also, a OH-PLIF measurement system is used to obtain instantaneous OH radical distribution. The OH-PLIF measurement system consists of an Nd:YAG laser (Continuum, Surelite III; wavelength: 532 nm, intensity: 70 mJ/pulse, frequency: 10 Hz, pulse duration: 7 ns), a dye laser (Radiant Dyes, Narrow Scan; wavelength: 283.92 nm, intensity: 4.8 mJ/pulse) with a frequency doubler, a digital delay generator (Quantum Composers, 9514 plus) and an ICCD camera as shown in Fig. 1b. The effective height of the laser sheet is approximately 40 mm, and the resolution of OH^* chemiluminescence and OH-PLIF images is 25.0 μm/pixel.

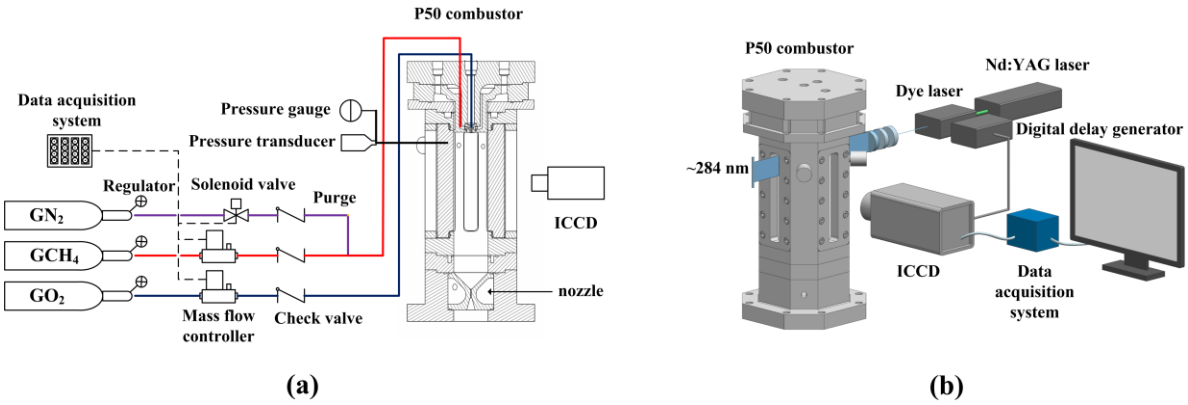

Figure 1: Schematics of experimental apparatus (a) and OH-PLIF imaging system (b).

3 Results and Discussion

Fig. 2 shows the OH^* distribution of the GO_2/GCH_4 coaxial jet flames in the model combustion chamber at opened (a) and 1.0 mm (b) nozzle conditions: the O_2 and CH_4 Reynolds numbers Re_O = 6,196–21,069 and Re_F = 1,064–3,619 at $(O/F)_{mom}$ = 6.0, which correspond to the stable anchored flame condition. For the fully opened nozzle and Re_O > 21,069 condition, the stable anchored flame is switched to a near-blowout flame which is lifted and oscillating upward and downward. Thus, the OH^* distribution is obtained only for the stable anchored flames as well as the flames of the same Re at the 1.0 mm nozzle condition. P_c is 1.0 bar for all the fully opened nozzle conditions and elevated for the 1.0 mm nozzle conditions. The elevated P_c is indicated for each image in Fig. 2b. The left side of each image in Fig. 2 is the LOS OH^* chemiluminescence image and the right side is the planar OH^* chemiluminescence image that is converted from the corresponding LOS image by the inverse Abel transform [14]. Each LOS image (7.5 × 25.6 mm^2) is obtained by averaging 50 images with the exposure time of 10 and 2 ms respectively for the fully opened nozzle and 1.0 mm nozzle conditions to prevent the saturation of OH^* chemiluminescence signal. For the fully opened nozzle condition, the OH^* distribution near the injector lip is changed at Re_O = 21,069, which is indicated by the white arrow, because local flame extinction frequently occurs at the corresponding region, which will be clearly confirmed in the OH-PLIF images (Fig. 4). The OH^* intensity generally increases with increasing P_c, which is expected to be caused by the increase of flame temperature and density [15]. Also, the enhanced P_c at a fixed value of Re causes the decrease of injection velocity of reactants compared with the fully opened nozzle conditions, which would reduce the local strain rate that affects the intensity of OH^* chemiluminescence signals [16]. Thus, the intensity in the region that is indicated by the white arrow in Fig. 2a is relatively high at the 1.0 mm nozzle condition compared with the fully opened nozzle conditions.

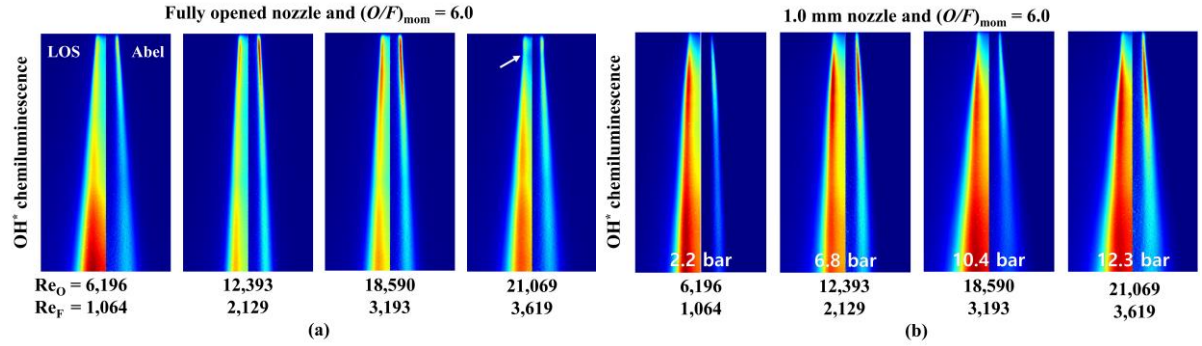

Figure 2: OH^* distribution for GO_2/GCH_4 coaxial jet flames at fully opened (a) and 1.0 mm (b) nozzle conditions.

Fig. 3 shows the location where the maximum OH^* intensity is found in the planar images of Fig. 2, L_f, in terms of Re_O. In general, L_f slightly increases with increasing Re_O. This tendency seems to be observed due to the enhanced local vorticity and strain rate in the region close to the injector lip, which attenuate the OH^* intensity [16]. For Re_O = 21,069 at the fully opened nozzle condition, however, L_f decreases due to the occurrence of local flame extinction, which will be confirmed in Fig. 4. With enhanced P_c for the 1.0 mm nozzle condition, L_f increases compared with the fully opened nozzle conditions since the reduced local strain rate at a fixed value of Re_O induces higher OH^* intensity and stable burning near the region that is indicated by the white arrow in Fig. 2 instead of the occurrence of local flame extinction.

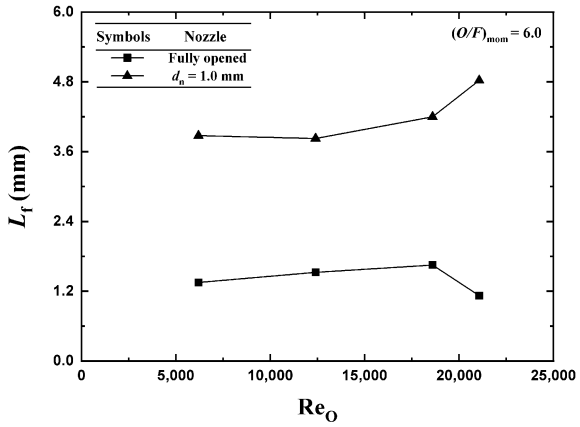

Figure 3: Location for maximum OH^* intensity (L_f) in GO_2/GCH_4 coaxial jet flames of Re_O = 6,196–21,069, Re_F = 1,064–3,619 and $(O/F)_{mom}$ = 6.0 at fully opened and 1.0 mm nozzle conditions.

Fig. 4 shows OH-PLIF images for the GO_2/GCH_4 coaxial jet flames in the model combustion chamber at opened (a) and 1.0 mm (b) nozzle conditions. With increasing Re_O, the flame wrinkling increases and the OH layer thickness generally decreases due to the enhanced local vorticity and strain rate [17]. For Re_O = 18,590–21,069 at the fully opened nozzle condition, the local flame extinction is confirmed by the disconnected OH distribution which is indicated by the white arrow in the figure. The occurrence of local flame extinction is enhanced by increasing Re due to the enhanced local vorticity and strain rate [18,19], but it is suppressed by increasing P_c since the decrease of injection velocity of reactants reduces the local strain rate compared with the fully opened nozzle conditions at a fixed value of Re_O. With increasing P_c, the OH intensity is enhanced and its distribution becomes more scattered due to the enhanced density and the slow recombination of OH radicals, though the enhanced collisional quenching and the broadening of OH absorption line shape would reduce it [20,21].

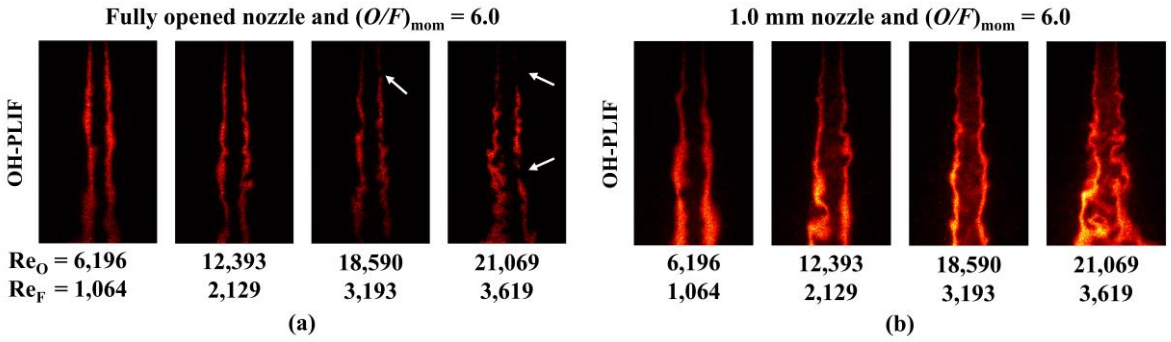

Figure 4: OH-PLIF images of GO_2/GCH_4 coaxial jet flames at opened (a) and 1.0 mm (b) nozzle conditions.

4 Conclusion

Fundamental combustion characteristics of GO_2/GCH_4 coaxial jet flames in a model combustion chamber at elevated combustion pressure up to 12.3 bar have been investigated through the flame visualization such as OH^* chemiluminescence and OH-PLIF imaging. In this study, only stable anchored flames were considered at various combustion pressure conditions. The OH^* chemiluminescence intensity increases with increasing combustion pressure, and the location where the maximum OH^*

intensity is found moves downward with increasing Re_O and combustion pressure, but it moves closer to the injector lip in the case that local flame extinction occurs. OH-PLIF images exhibit that the flame wrinkling increases and the OH layer thickness generally decreases with increasing Re, the occurrence of local flame extinction is confirmed by the disconnected OH distribution and it is suppressed with enhanced combustion pressure. Also, the OH intensity is enhanced and its distribution becomes more scattered with increasing combustion pressure, due to the enhanced density and the slow recombination of OH radicals, though the enhanced collisional quenching and the broadening of OH absorption line shape would reduce it.

Acknowledgment

This work was supported by the National Research Foundation of Korea (NRF) and the Korea Evaluation Institute of Industrial Technology (KEIT) funded by the Korea government (MSIT and MOTIE) (NRF-2021R1A2C2005644 and RS-2022-00155546).

References

[1] Mehendiratta D, Ramachandran M. (2018). A review on different propellant materials for space vehicles and their characterization. Int. J. Mech. Prod. Eng. Res. Dev. 93.

[2] Burkhardt H, Sippel M, Herbertz A, Klevanski J. (2004). Kerosene vs methane: A propellant tradeoff for reusable liquid booster stages. J. Spacecraft Rockets. 41:762.

[3] Gotz A, Mading C, Brummer L, Haeseler D. (2001). Application of non-toxic propellants for future launch vehicles. AIAA-2001-3546.

[4] Klepikov IA, Katorgin BI, Chvanov VK. (1997). The new generation of rocket engines, operating by ecologically safe propellant "liquid oxygen and liquefied natural gas(methane)". Acta Astronaut. 41:209.

[5] Theron M, Benito MM, Vieille B, Vingert L, Fdida N, Mauriot Y, Blouquin R, Seitan C, et al. (2019). Experimental and numerical investigation of LOx/methane cryogenic combustion at low mixture ratio. 8th European Conference for Aeronautics and Space Sciences.

[6] Son M, Lee KW, Koo JY. (2020). Characteristics of anchoring locations and angles for GOx/GCH_4 flames of an annular pintle injector. Acta Astronaut. 177:707.

[7] Kim TY, Choi S, Kim HK, Jeung IS, Koo J, Kwon OC. (2016). Combustion properties of gaseous CH_4/O_2 coaxial jet flames in a single-element combustor. Fuel 184:28.

[8] Choi S, Kim TY, Kim HK, Jeung IS, Koo J, Kwon OC. (2017). Combustion stability of gaseous CH_4/O_2 and H_2/O_2 coaxial jet flames in a single-element combustor. Energy 132:57.

[9] Kim TY, Choi S, Kim YH, Ahn YJ, Kim HK, Kwon OC. (2018). Combustion characteristics of gaseous inverse O_2/H_2 coaxial jet flames in a single-element model combustor. Energy 155:262.

[10] Kim TY, Kim YH, Ahn YJ, Choi S, Kwon OC. (2019). Combustion stability of inverse oxygen/hydrogen coaxial jet flames at high pressure. Energy 180:121.

[11] Choi S, Kim YH, Kim TY, Kwon OC. (2022). Localized combustion phenomena of inverse nonpremixed pure O_2/CH_4 coaxial jet flames at near-limit conditions. Combust. Sci. Technol. Advance online publication. https://doi.org/10.1080/00102202.2022.2155813

[12] Moore JD, Kuo KK (2008). Effect of switching methane/oxygen reactants in a coaxial injector on the stability of non-premixed flames. Combust. Sci. Technol. 180:401.

[13] Abada O, Abada A, El-Hirtsi AA (2020). Effect of bipropellant combustion products on the rocket nozzle design. Mech. Ind. 21:515.

[14] Yuan ZG (2003). The filtered Abel transform and its application in combustion diagnostics. Cleveland, OH, USA; NASA. CR-2003-212121.

[15] Fiala T. (2015). Radiation from high pressure hydrogen-oxygen flames and its use in assessing rocket combustion instability. Munich, Germany: Ph.D. thesis, Technical University of Munich.

[16] Ayoola BO, Balachandran R, Frank JH, Mastorakos E, Kaminski CF (2006). Spatially resolved heat release rate measurements in turbulent premixed flames. Combust. Flame 144:1.

[17] Peters N. (1986). Laminar flamelet concepts in turbulent combustion. Proc. Combust. Inst. 21:1231.

[18] Hult J, Meier U, Meier W, Harvey A, Kaminski CF. (2005). Experimental analysis of local flame extinction in a turbulent jet diffusion flame by high repetition 2-D laser techniques and multi-scalar measurements. Proc. Combust. Inst. 30:701.

[19] Kyritsis DC, Santoro VS, Gomez A. (2002). Quantitative scalar dissipation rate measurements in vortex-perturbed counterflow diffusion flames. Proc. Combust. Inst. 29:1679.

[20] Singla G, Scouflaire P, Rolon C, Candel S. (2006). Planar laser-induced fluorescence of OH in high-pressure cryogenic LO_x/GH_2 jet flames. Combust. Flame 144:151.

[21] Vaidyanathan A, Gustavsson J, Segal C. (2009). Oxygen/hydrogen-planar-laser-induced fluorescence measurements and accuracy investigation in high-pressure combustion. J. Propuls. Power. 25:864.